Influence of the urban environment on the effectiveness of natural night-ventilation of an office building

Rubina Ramponi [a,b], Isabella Gaetani [c], Adriana Angelotti [c,*]

[a] *Architecture, Built Environment, Construction Engineering Department, Politecnico di Milano, via Ponzio 31,20133 Milano, Italy*
[b] *Building Physics and Services, Eindhoven University of Technology, P.O. box 513, 5600 MB Eindhoven, the Netherlands*
[c] *Energy Department, Politecnico di Milano, via Lambruschini 4, 20156 Milano, Italy*

Received 6 August 2013
Received in revised form 7 February 2014
Accepted 1 April 2014
Available online 13 April 2014

1. Introduction

Natural night-ventilation is an important passive cooling technique for reducing summer energy consumption in the built environment [1]. The cooling effect is achieved by combining natural night-ventilation with the high thermal inertia of the building structure [2–4]. In fact, the building structure acts as heat storage during the day and releases the absorbed heat during the night, when the cooling effect of natural ventilation is leading [5]. Besides the thermal properties of the building structure, the cooling potential of natural night-ventilation is strongly affected by the local climate. The latter is the result of meteorological conditions, the effect of urban morphology and other microclimatic variables, e.g. environmental albedo or the Urban Heat Island (UHI) effect. The UHI effect is caused, among other things, by the combined effect of urban geometry, thermal properties of the surfaces, the anthropogenic heat, the greenhouse effect and the emissivity of the surfaces [6].

The influence of the meteorological conditions on the cooling potential for night-ventilation depends on the combined impact of night-time wind speed and air temperature. Whereas the outdoor wind speed and profile affects the ventilation rate across the building, the outdoor night temperature represents the heat sink temperature for the building heat dissipation. The importance of the local outdoor temperature level is pointed out by Artmann et al. [7], who defined a Climatic Cooling Potential (CCP) index based on the indoor-outdoor night temperature differences. The CCP index aims to identify the suitability of the climate for night cooling. For instance, the CCP map of Europe [7] shows high potential for night-cooling over the whole of Northern Europe and still significant potential in Central, Eastern and even in some regions of Southern Europe.

In addition to the meteorological conditions, local climatic modifications primarily due to the urban morphology affect the night-cooling potential. On the one hand, the presence of adjacent buildings has a beneficial solar shading effect during the cooling season. On the other hand, the wind shielding effect of the surrounding buildings alters the wind pressure distribution on the envelope and reduces the ventilation rates [8,9]. The wind flow within the urban canyons is strongly influenced by the urban

* Corresponding author. Tel.: +39 02 23995183.
E-mail address: adriana.angelotti@polimi.it (A. Angelotti).

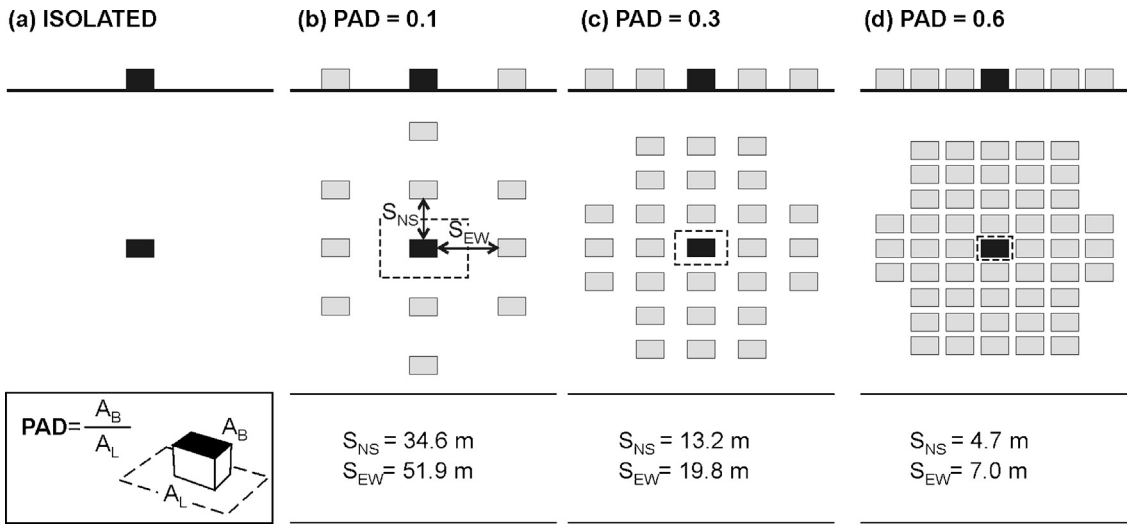

Fig. 1. Top view of the cases analyzed, i.e. isolated reference building (a), PAD 0.1 (b), 0.3 (c), and 0.6 (d); definition of the PAD and size of the streets along the North–South (S_{NS}) and East–West (S_{EW}) direction.

morphology which is described by the building packing density and building arrangement. Various morphological parameters are used to measure the building packing density either focusing on the street canyon scale or on the neighborhood scale [10–12]. The building and the canyon aspect ratios are often used at street canyon scale, while the Plan (PAD) and Frontal (FAD) Area Densities are defined for the neighborhood scale. The PAD represents the ratio between the plan (A_B) and the lot area (A_L), as in Fig. 1 (a), while the FAD is defined as the ratio between the frontal (A_F) area of the building and the lot area (A_L). At increasing Plan and Frontal Area Densities, the main flow goes from an isolated flow regime, to a wake interference flow regime, to a skimming flow regime [11,12], affecting the wind-pressure on the building facades.

The impact of urban morphology on the cooling demand of buildings can be estimated using Building Energy Simulation (BES) tools with embedded Airflow Network (AFN) models to predict the natural ventilation contribution from the wind pressure on the building envelope [13–15]. Weather datasets were developed to represent local climatic conditions in BES simulations and can be modified to take into account different climatic scenarios, such as the UHI effect [16,17]. As regards to the urban morphology, the solar shading of adjacent buildings can be explicitly modeled, but the variation of the wind-pressure on the building surfaces is rather difficult to model. Pressure coefficients for non-isolated buildings can be extracted from external databases, measurements, or numerical models [18–20]. However, the latter two are considered more reliable as they are able to model similar geometric and wind conditions [18].

In spite of their strong counteracting influence on the energy performance of a non-isolated building, most of the past studies addressed the effects of the solar shading and the wind shielding separately. Among others, van Moeseke et al. [9] and Schulze and Eicker [21] analyzed the impact of the local wind modifications due to the urban environment using BES/AFN tools. Van Moeseke et al. [9] evaluated natural ventilation rates in an office building in Uccle, Belgium, for a typical summer day. During the simulation day, constant wind speed and direction were assumed, but the upstream wind profile as well as the C_p values on the building facades varied to reproduce an open, a suburban and an urban environment which caused significant reductions in the Air Changes per Hour (ACH) for given wind incident angles. Similarly, Schulze and Eicker [21] calculated the monthly average ACH for different natural ventilation strategies in an office building and found that the average ACH values obtained for purely wind-driven cross-ventilation vary from 11.7 to 8.0 and to 4.7 h^{-1} assuming an upstream wind profile for country, urban and city terrain, respectively. A different approach to assess the cooling potential of night-ventilation is proposed by Geros et al. [2], who used experimental wind field and air temperature data measured inside and outside ten urban street canyons in Athens (Greece) as boundary conditions for BES/AFN simulations. The energy performance of a single-zone room located inside and outside the canyons shows an overestimation of the cooling efficiency of night ventilation when undisturbed climatic conditions outside the canyon are used. Finally, the impact of solar shading by adjacent buildings on the heating/cooling demand is studied with BES tools, e.g. by [22–24]. Results are clearly climate-dependent, but in general a significant influence is found, meaning that the solar shading of the surrounding obstacles should be included. In conclusion, to the best of the authors' knowledge, there is a lack of systematic studies that consider both wind shielding and solar shading effects in the urban environment and evaluate their combined impact on the cooling energy savings for natural night-ventilation.

The present study provides a systematic analysis of the impact of the urban environment on the effectiveness of natural night-ventilation for a low-rise office building (reference building). The reference building is analyzed as isolated and as placed in the center of simplified urban areas composed of uniform buildings of Plan Area Density (PAD) equal to 0.1, 0.3 and 0.6. These PAD values were chosen to consider different urban wind flow regimes [12] but also to take into account realistic obstruction distances [24]. The energy demand of the reference building and the natural ventilation effectiveness are evaluated with EnergyPlus and the embedded AFN model [25]. The validity of the integration of EnergyPlus with the AFN model for natural ventilation has been reported in previous studies [13,26]. Applications of BES/AFN tools to evaluate the effect of the urban environment on the energy performance of non-isolated buildings are still rather limited. In this study, the geometry and albedo properties of the surrounding buildings are explicitly modeled to consider the solar shading effect on the reference building. Furthermore, the impact of building packing density on the wind velocity profile is taken into account by adopting experimental wind pressure coefficients achieved by Quan et al. [27,28]. Finally, the influence of the local weather is assessed by considering

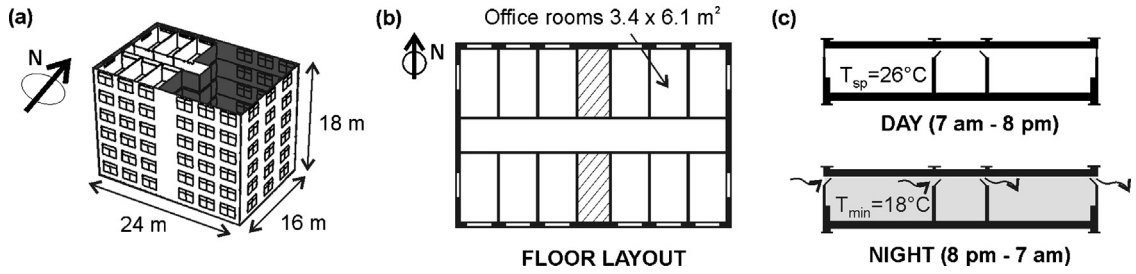

Fig. 2. (a) Building geometry and (b) plan of a typical floor layout (in white the occupied zones), and (c) schedule of the natural ventilation system. During the day, the building is unventilated and a set point temperature (T_{sp}) of 26 °C is imposed; during the night, the windows are open and a minimum indoor temperature (T_{min}) of 18 °C is set to avoid excessive cooling.

three European locations of different climate suitability for night-cooling, and a simplified UHI scenario [16] is implemented for sensitivity analyses.

At first, the impact of the solar shading of the surroundings is investigated in terms of variation of cooling demand of the unventilated building with the PAD at different locations. The sensitivity to the albedo of the adjacent surfaces and to the UHI scenario is also assessed. Then, the influence of wind shielding by neighboring buildings is analyzed with the night-ventilation rates and the relative ventilation losses for different PAD values at different locations. Finally, the overall effect of both aspects characterizing the urban environment is studied by considering the energy savings of the night ventilated building at increasing PAD. Since the effects of solar shading and wind shielding are expected to vary with the floor elevation, the 2nd and the 5th floors of the building are simulated and the results are compared and discussed.

2. Materials and methods

2.1. Characteristics of the building

The reference building is a six-story office building with the dimensions of $24 \times 16 \times 18$ m^3, subjected to cross-ventilation (Fig. 2a). In each floor of the building, 12 office rooms of $3.4 \times 6.1 \times 2.7$ m^3 and two service rooms are aligned on the northern and southern sides of a corridor, as in Fig. 2b. Large non-operable windows equipped with external shading devices are placed on the external walls of the office rooms and are sized 2.4×1.2 m^2. Above these, bottom-up operable windows of 2.4×0.6 m^2 allow cross-ventilation in combination with internal operable windows of 3.4×0.6 m^2 located above the doors facing the corridor (Fig. 2c).

The construction materials of the building structure are assembled to improve thermal inertia and are summarized in Table 1. In order to evaluate the response of the components to the variation of the outdoor and indoor temperature, periodic thermal transmittance and internal admittance are calculated with their associated time lag and time lead. The calculation is performed according to CEN EN ISO 13786 [29], as in [30,31] and results are reported in Table 1. Double pane low-emissivity windows filled with Argon are used for the external glazed surfaces, characterized by a U-value of 2.46 W/(m^{2}K) and a Solar Heat Gain Coefficient (SHGC) of 0.45. Solar shading devices on the external windows are activated when the solar radiation incident on the window exceeds 300 W/m^2.

The building is occupied from 7 a.m. to 6 p.m. in weekdays (Monday to Friday). The internal heat gains are assumed for the occupied and unoccupied period in accordance with the Italian standard UNI/TS 11300-1 [32]. During occupancy, the internal gains are equal to 20 W/m^2 and 8 W/m^2 in the office rooms and in the corridor, respectively. During night, weekend and other unoccupied periods, the internal heat gains are reduced to 2 W/m^2 and 1 W/m^2 in the office rooms and the corridor, respectively.

Simulations are performed during the cooling season that runs from June to September. During this period, an ideal mechanical cooling system is active in weekdays from 7 a.m. to 6 p.m. to keep the indoor temperature below the set-point value (T_{sp}) of 26 °C [32]. At night, external windows are opened to about 20° from the vertical to allow natural ventilation, and closed if the indoor temperature drops below 18 °C to avoid excessive cooling. The internal windows remain open 24 hours at 45° to improve the circulation of the indoor airflow.

2.2. Characteristics of the urban environment

The reference building considered for the analyses is either isolated or located in the center of urban areas with PAD increasing from 0.1, to 0.3, to 0.6 (Fig. 1). As a result, the street widths along the two orientations (S_{NS}, S_{EW}) are varying as listed in Fig. 1. The urban areas are composed of buildings with the same geometry as the reference building. A uniform albedo is set to 0.3 (medium darkly colored surfaces) for all the surfaces of the surrounding buildings in the baseline case, and is increased to 0.7 (lightly colored surfaces) in the sensitivity test (albedo 0.7 scenario). A ground albedo of 0.2 is assumed for the street canyons. The surrounding terrain, whose roughness influences the development of the upstream wind profile, is taken as suburban [33] for all the cases analyzed. Further information about the wind profile is provided in Sect. 2.3.

Table 1
Composition and thermal properties of the building structure.

		Periodic thermal transmittance			Internal admittance	
		U-value	Amplitude	Time lag	Amplitude	Time lead
Wall	Composition (inside to outside)	[W/(m^{2}K)]	[W/(m^{2}K)]	[h]	[W/(m^{2}K)]	[h]
External wall	2 cm plaster, 24 cm brick masonry, 8.5 cm polystyrene, 2 cm plaster	0.34	0.04	−11.04	3.96	1.27
Ceiling	1.2 cm cement building board, 15 cm cast concrete, 5 cm screed, 1 cm carpet/underlay	2.04	–	–	5.17	1.11
Floor	1 cm carpet/underlay, 5 cm screed, 15 cm cast concrete, 1.2 cm cement building board	2.04	–	–	4.25	1.19
Partitions	1.3 cm plaster, 16 cm brick masonry, 1.3 cm plaster	1.45	–	–	3.51	1.17

Table 2
Night-averaged air temperature ($T_{out,N}$), wind speed (U_N) and cooling degree hours (CDH) for Amsterdam (AM), Milan (MI) and Rome (RO) during the period of interest (Jun–Sept).

Location	Night-averaged air temperature ($T_{out,N}$)	Night-averaged wind speed (U_N)	Cooling-degrees hour (CDH)
	[°C]	[m/s]	[°C h]
Amsterdam (AM)	14.0	3.5	154
Milan (MI)	17.7	0.5	815
Rome (RO)	20.4	2.1	1044

The cases under study are located in three different European locations: Amsterdam (The Netherlands), Milan (Italy) and Rome (Italy). Table 2 shows the climatic variables influencing the night-cooling suitability for the three locations during the period of interest (Jun-Sept), i.e. night-averaged outdoor air temperature and wind speed, calculated from IWEC weather data for typical meteorological years [34]. It can be noticed that Amsterdam (AM) is characterized by a very low night-averaged air temperature of 14 °C and a high wind speed of 3.5 m/s. On the contrary, Milan and Rome have relatively high night-averaged air temperatures of 17.7 °C and 20.4 °C, respectively, but very different wind speeds from 0.5 m/s in Milan to 2.1 m/s in Rome. Table 2 reports also the Cooling Degree Hours (CDH) [35] for the three locations, namely:

$$CDH = \sum_{k=1}^{N_{hours}} (T_{out,k} - T_{sp,k}) \quad with\, T_{out,k} - T_{sp,k} > 0 \tag{2}$$

where $T_{out,k}$ is the outdoor air temperature at hour k, and $T_{sp,k}$ is the indoor design set-point temperature, i.e. 26 °C in this paper. The CDH can be used as an indicator of the cooling energy demand in a given climate, although it should be noted that this value is also influenced by solar gains.

2.3. Thermal and ventilation model

The reference building is modeled using EnergyPlus [25] assigning a different thermal zone to each room, so that each floor results in 14 thermal zones (Fig. 2b). The simulations are performed for the 2nd and 5th floor of the building, chosen to investigate the effect of the floor elevation without the influence of the ground and roof level boundary conditions. In order to reduce the computational effort, each floor is simulated separately and adiabatic slabs are assumed for the intermediate floors. This assumption implies that the heat flow between adjacent floors across the slabs is negligible. During daytime, this is the case when the mechanical cooling system maintains the same temperature in the two floors across the slab. However, this assumption is considered valid also during daytime when the mechanical cooling system is not active and during nighttime. In fact, the heat exchange with the outdoor environment is expected to have a higher impact on the zone air balance than the heat exchange across the slab, especially during nighttime, in the absence of internal and solar heat gains. The thermal properties of the building structures, as well as the occupancy profiles and the internal gains are as described in Section 2.1. The mechanical air cooling system is defined using the ideal air cooling system defined by EnergyPlus (Ideal Load HVAC system [25]). The Ideal Load HVAC system is an ideal VAV terminal unit with variable supply temperature and humidity; the supply air flow rate varies between zero and the maximum in order to satisfy the zone cooling load for the given set-point temperature of 26 °C.

The surrounding buildings are modeled in EnergyPlus through the definition of opaque shading surfaces with given albedo characteristics. Therefore, only the surfaces adjacent to the reference building are explicitly modeled, as shown in Fig. 3.

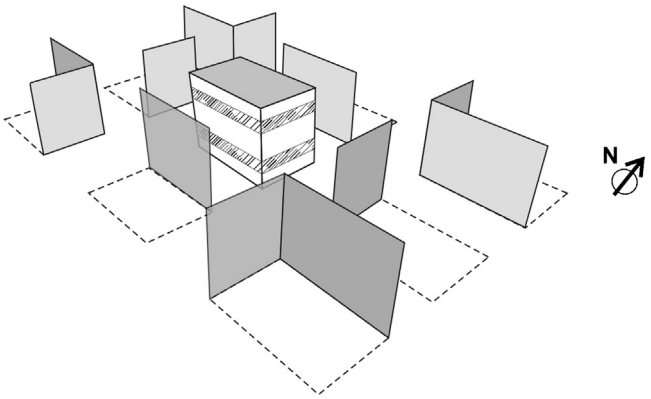

Fig. 3. The reference building and the adjacent buildings shading surfaces in EnergyPlus model.

Airflow simulations are carried out using the AFN model embedded in EnergyPlus. In the AFN approach, a mass balance within several zonal nodes connected by airflow elements, e.g. openings, doors, or cracks, is performed. Each zonal node is characterized by temperature and pressure conditions, while correlations between pressure difference and airflow are assigned to the airflow elements. Boundary conditions for natural ventilation are imposed at the external nodes by means of wind pressure coefficients on the building envelope. The external and internal openings are modeled as large vertical openings characterized by a given discharge coefficient.

The pressure coefficients (C_p) relate the static pressure P_x at a given point on the building facade to a reference wind speed U_{ref} as in Eq. (2):

$$C_p = \frac{P_x - P_{ref}}{0.5\rho U_{ref}^2} \tag{2}$$

where ρ is the air density and P_{ref} is the reference static pressure measured at a reference height in the upstream undisturbed flow. C_p values are strongly related to the building characteristics (geometry and façade design); the geometry and arrangement of the surrounding obstacles; and the wind profile and incidence angle. The set of C_p values used in this study are extracted from the measurements performed by Quan et al. [27,28] on reduced-scale urban configurations with the same geometry and arrangement as the cases considered in this study. Furthermore, the wind profile imposed in the BES/AFN model was chosen in accordance with the measured wind incident profile corresponding to a suburban terrain type (Cat. III of AIJ standard [33]). The wind-tunnel profile was characterized by an exponent $\alpha = 0.2$ and a gradient height $\delta = 450$ m and the pressure coefficients were calculated with respect to a reference wind speed at 0.1 m height (reduced-scale). In the BES/AFN model simulations, the local wind profile is derived from the wind profile at the meteorological station as in Eq. (3) [25,36]:

$$U(z) = U_{met}\left(\frac{\delta_{met}}{z_{met}}\right)^{\alpha_{met}}\left(\frac{z}{\delta}\right)^{\alpha} \tag{3}$$

where $U(z)$ is the local wind speed, U_{met} is the wind speed measured at the meteorological station (m/s) and $\alpha_{met} = 0.14$ and $\delta_{met} = 270$ m are the characteristics of the open-terrain wind profile at the meteorological station.

In the AFN modeling carried out in this study, the external operable windows connect the external pressure nodes on the building facades to the internal (zonal) nodes in the office rooms and are characterized by a discharge coefficient of 0.6 [1]. The internal windows, connecting the office rooms with the corridor, have a discharge coefficient of 0.78 [1].

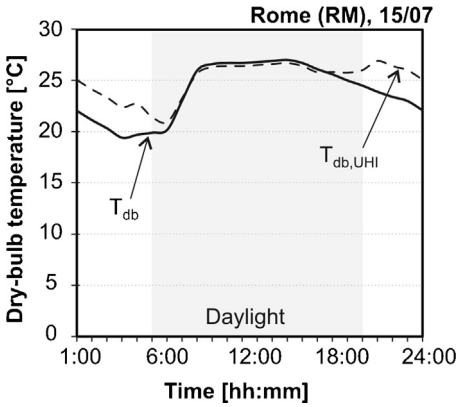

Fig. 4. Dry bulb temperature in Rome (RM) on July 15th as measured (T_{db}) in an open-field location and modified ($T_{db,UHI}$) according to [16] with ΔT_{db} equal to 3 °C.

2.4. Modification of the weather files

Meteorological data from the International Weather for Energy Calculation (IWEC) database [34] were used in the simulations. The IWEC data are referred to as a Typical Meteorological Year and collect measurements from open field locations neglecting the effect of the UHI. Although an accurate modeling of the UHI effect is beyond the scope of this study, a simplified UHI scenario was created as in the model proposed by Crawley [16]. According to [16], a modified daily pattern of dry bulb temperature $T_{db,UHI}$ due to the UHI is defined from the measured dry bulb temperature T_{db} and a maximum increment ΔT_{db}, ranging from 1 °C to 5 °C, as in Eq. (4):

$$T_{db,UHI} = T_{db} + k\Delta T_{db} \quad (4)$$

The value of k (Eq. (4)) varies according with the time of the day, being equal to 1 during the night, 0.5 at the first or last hour of daylight, 0.25 at the second and next to last hour of daylight, 0.0755 at the third and second to last hour of daylight, and −0.1 otherwise. For the present case, modified weather data are defined for each location with ΔT_{db} equal to 3 °C and used in the BES/AFN simulations to test the influence of a simplified UHI scenario on the energy savings for night-ventilation. Fig. 4 shows an example of the measured (T_{db}) and modified ($T_{db,UHI}$) dry bulb temperature for a summer day in Rome (July 15th).

A summary of the variables and characteristics of the baseline case and the albedo 0.7 and simplified UHI scenarios analyzed in the present study is reported in Fig. 5. It has to be pointed out that the albedo 0.7 scenario and the simplified UHI scenario have been applied only to the high density urban environments, namely PAD 0.3 and 0.6.

Table 3
Aspects considered in each phase of the analysis and related indicators.

Aspects analyzed	Indicators	
Solar shading by adjacent buildings (Section 3.1)	Seasonal solar energy transmitted through the windows	T_{SOL} [kwh/m^2]
	Seasonal cooling energy demand of the unventilated building	$Q_{C,UV}$ [kwh/m^2]
Wind shielding by adjacent buildings (Section 3.2)	Night-averaged ventilation rates	ACH_N [h^{-1}]
	Seasonal night ventilation losses	Q_V [kwh/m^2]
Influence of the urban environment (Section 3.3)	Seasonal cooling energy demand of the night-ventilated building	$Q_{C,V}$ [kwh/m^2]
	Seasonal energy savings	ES [%]

3. Results and remarks

The impact of the urban environment on the cooling effectiveness of natural night-ventilation is evaluated considering the combined solar shading and wind shielding effects of the surroundings on the cooling energy savings of the night-ventilated reference building.

The solar shading by adjacent buildings is first evaluated for the unventilated building considering the variation of the solar energy transmitted through the windows and the related cooling demand with the Plan Area Density and the floor elevation. The results are illustrated in Section 3.1. Then, the wind shielding of the surrounding buildings is evaluated for the night-ventilated building as the impact of the PAD on the ventilation rates through the windows and the ventilation losses due to night-ventilation. Results are shown and discussed in Section 3.2. Finally, the overall effect of the urban environment on the cooling energy demand of the night-ventilated building and the related energy savings are analyzed in detail. The combined solar shading and wind shielding effects of the adjacent buildings for different PAD, floor elevation, and local weather are investigated and the results are presented and discussed in Section 3.3. The aspects considered in each phase of the analysis are reported in Table 3 as well as the related indicators.

3.1. Effect of the solar shading by adjacent buildings

The solar shading caused by adjacent buildings is analyzed for the unventilated building. In particular, the solar energy transmitted (T_{SOL}) through the windows and the cooling energy demand ($Q_{C,UV}$) are calculated in each thermal zone by varying PAD, floor elevation and location. Fig. 6 shows the mean values of T_{SOL} and $Q_{C,UV}$ over the simulation period for the baseline case and Table 4

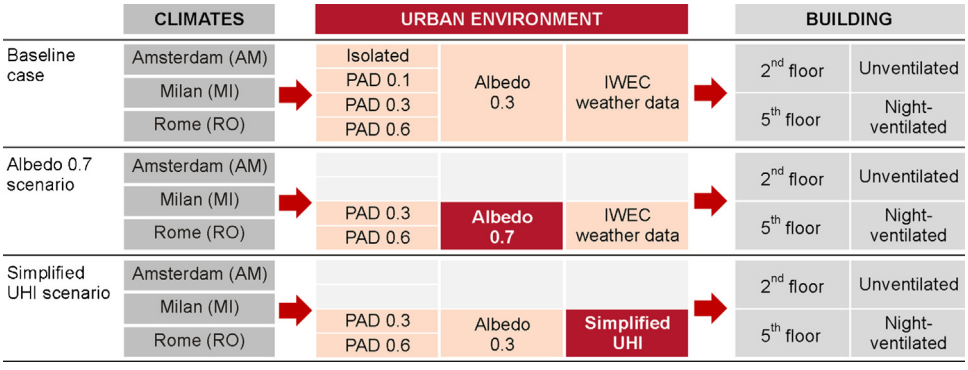

Fig. 5. Variables and characteristics of the baseline case and the albedo 0.7 and simplified UHI scenarios analyzed in the present study.

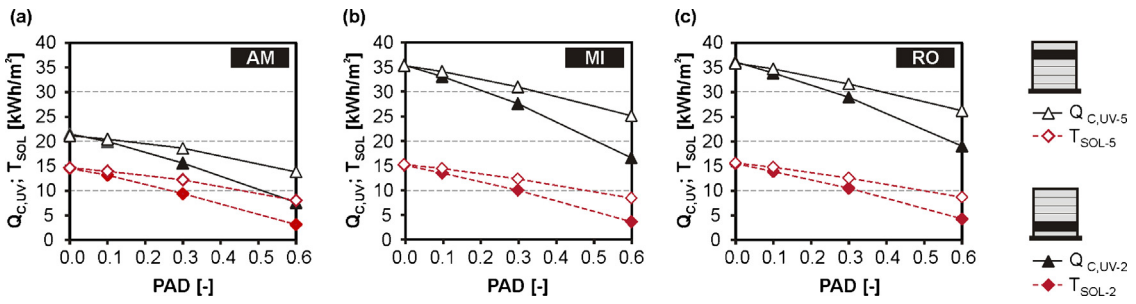

Fig. 6. Transmitted solar energy through windows (T_{SOL}) and cooling energy demand ($Q_{C,UV}$) of the unventilated building versus PAD for the 2nd and the 5th floor in (a) Amsterdam; (b) Milan; (c) Rome.

lists the mean and standard deviation obtained from the different thermal zones data. It can be noticed that the values and the behavior of T_{SOL} with the PAD are similar in the three locations, due to the effects of the solar shading devices installed on the windows. Overall, the reduction of T_{SOL} with the PAD varies with the floor elevation and is stronger at the 2nd floor, being already evident at PAD = 0.1. For instance, in Amsterdam (Fig. 6a and Table 4) T_{SOL} is reduced by 10% at the 2nd floor and by 5% at the 5th floor at PAD = 0.1 with respect to the isolated building. Higher reductions with respect to the isolated building are shown at increased PAD values, with a maximum of about 79% at the 2nd floor and 46% at the 5th floor for PAD = 0.6. Similar trends are reported for Milan and Rome in Fig. 6 and Table 4.

In spite of the similar solar gains, the cooling energy demands at the three locations (Fig. 6, Table 4) differ significantly, as a consequence of the relative importance of the heat gains through the envelope due to the outdoor-indoor temperature difference. In fact, while in Amsterdam (Fig. 6a) the solar gains play a major role in the cooling energy demand, Milan (Fig. 6b) and Rome (Fig. 6c) register very high diurnal temperatures that increase the cooling demand. The effect of the indoor–outdoor temperature difference on the cooling energy demand is also evident in the CDH, which are equal to 154 in Amsterdam, and 815 and 1044 in Milan and Rome, respectively (Table 2). Overall, the reduction of $Q_{C,UV}$ with the PAD and the floor elevation (Fig. 6, Table 4) shows the influence of the decreased solar energy transmitted through the windows in each location. When passing from the isolated case to PAD = 0.1 the impact on the cooling energy demand is very small, especially at the 5th floor where the reduction of T_{SOL} is less significant. For instance, when considering Amsterdam (Fig. 6a) $Q_{C,UV}$ is reduced by about the 7% at the 2nd floor and by 3% at the 5th floor at PAD = 0.1 compared to the isolated building. The differences among the three locations are more remarkable for higher PAD values. In particular, at PAD = 0.6 the impact of the solar shading is very important, leading to a reduction in $Q_{C,UV}$ equal to 65% (AM), 53% (MI) and 47% (RO) with respect to the isolated building at the 2nd floor and equal to 35% (AM), 29% (MI) and 27% (RO) at the 5th floor in the three locations.

Furthermore, Table 4 illustrates the effect of two additional scenarios on the cooling energy demand of the unventilated building. In the first scenario (Albedo 0.7), the albedo of the surrounding buildings is increased from 0.3 (Baseline case) to 0.7. As a consequence, the impact of the PAD on the solar energy transmitted through windows and on the cooling energy demand of the unventilated building is reduced. This condition occurs because the shading of the direct and sky diffuse solar radiation introduced by adjacent buildings is partially compensated by the increase in the solar radiation reflected from them. For instance, in Amsterdam at PAD = 0.6 T_{SOL} is reduced by 67% and by 30% with respect to the isolated building, at the 2nd and 5th floors respectively. Similar results are obtained for the other locations: the reduction of T_{SOL} at PAD = 0.6 is 61% and 26% in Milan as well as 58% and 26% in Rome, at the 2nd and 5th floors respectively. At the same time, the effect of PAD = 0.6 on $Q_{C,UV}$ in all the locations is a reduction of only 57% (AM), 46% (MI) and 40% (RO) at the 2nd floor, and 24% (AM), 18% (MI) and 17% (RO) at the 5th floor.

In the second scenario (Simplified UHI), the simplified UHI effect described in Section 2.4 is applied. In Table 4 the $Q_{C,UV}$ values obtained within the UHI scenario are reported. T_{SOL} is not affected by the UHI scenario and is therefore not reported. It can be noticed that the impact of the PAD on the cooling energy demand of

Table 4
Transmitted solar energy through windows (T_{SOL}) and cooling energy demand ($Q_{C,UV}$) for the unventilated building obtained with different PAD, locations and floor elevation (mean values and standard deviations over the thermal zones), for the baseline case and for the albedo 0.7 and the simplified UHI scenarios.

		Baseline case								Albedo 0.7 scenario								Simplified UHI scenario			
		T_{SOL} [kWh/m²]				Q_C [kWh/m²]				T_{SOL} [kWh/m²]				Q_C [kWh/m²]				Q_C [kWh/m²]			
		T_{SOL-2}		T_{SOL-5}		$Q_{C,UV-2}$		$Q_{C,UV-5}$		T_{SOL-2}		T_{SOL-5}		$Q_{C,UV-2}$		$Q_{C,UV-5}$		$Q_{C,UV-2}$		$Q_{C,UV-5}$	
		Mean	SD	Mean	SD	Mean	SD	Mean	SD	Mean	SD	Mean	SD	Mean	SD	Mean	SD	Mean	SD	Mean	SD
AM	isolated	14.4	6.7	14.5	6.7	21.4	4.1	21.1	3.9	–	–	–	–	–	–	–	–	–	–	–	–
	PAD 0.1	13.0	6.2	13.8	6.6	19.9	4.1	20.4	3.9	–	–	–	–	–	–	–	–	–	–	–	–
	PAD 0.3	9.3	5.5	12.1	6.0	15.5	3.2	18.5	3.6	11.0	6.0	13.8	6.6	17.3	2.9	20.4	3.3	16.7	3.4	19.8	3.8
	PAD 0.6	3.0	2.6	7.9	4.7	7.5	1.3	13.7	2.8	4.8	3.7	10.2	5.6	9.3	0.8	16.1	2.3	8.3	1.1	14.9	2.9
MI	isolated	15.2	7.3	15.3	7.4	35.5	8.8	35.4	8.6	–	–	–	–	–	–	–	–	–	–	–	–
	PAD 0.1	13.6	6.7	14.5	7.2	33.2	8.4	34.2	8.5	–	–	–	–	–	–	–	–	–	–	–	–
	PAD 0.3	10.1	5.9	12.4	6.5	27.7	6.9	31.1	7.7	12.1	6.5	14.4	7.2	30.2	6.9	33.6	7.8	28.9	7.1	32.3	7.9
	PAD 0.6	3.7	3.0	8.5	5.0	16.7	1.7	25.2	5.9	5.9	4.2	11.4	6.1	19.3	2.3	28.9	5.8	17.9	1.9	26.5	6.1
RO	isolated	15.6	7.5	15.7	7.6	36.3	8.5	36.0	8.3	–	–	–	–	–	–	–	–	–	–	–	–
	PAD 0.1	13.9	6.9	14.8	7.4	34.0	8.1	34.9	8.1	–	–	–	–	–	–	–	–	–	–	–	–
	PAD 0.3	10.5	6.1	12.6	6.7	29.1	6.9	31.8	7.4	12.5	6.8	14.6	7.5	31.5	7.0	34.2	7.6	30.4	7.1	33.1	7.7
	PAD 0.6	4.3	3.1	8.7	5.2	19.1	2.1	26.3	5.7	6.6	4.3	11.6	6.3	21.8	2.7	29.8	5.9	20.4	2.3	27.7	5.9

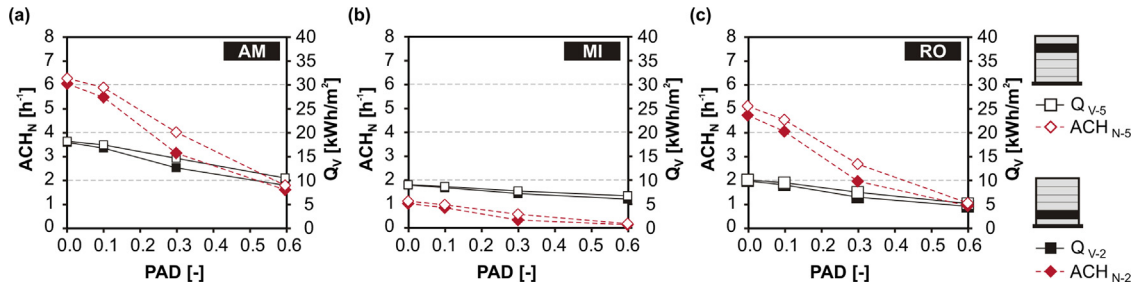

Fig. 7. Night-averaged Air Changes per Hour (ACH_N) and ventilation losses (Q_V) versus PAD for the 2nd and the 5th floor in (a) Amsterdam; (b) Milan; (c) Rome.

the unventilated building is slightly reduced with respect to the baseline case. In fact the reduction of solar gains due to adjacent buildings is partially compensated by the increase of the transmission gains associated with the higher night-temperature. At PAD = 0.6 $Q_{C,UV}$ in the three locations is reduced by 61% (AM), 50% (MI) and 44% (RO) compared to the isolated building at the 2nd floor, and by 29% (AM), 25% (MI) and 23% (RO) at the 5th floor.

This analysis remarks that Amsterdam shows the highest sensitivity of the cooling energy demand to the PAD, followed by Milan and Rome. These results are consistent with the fact that the building cooling energy demand in Amsterdam is dominated by the effect of solar and internal gains. Therefore, the reduction of the solar gains due to the increased PAD has a stronger impact in Amsterdam than in the other locations.

3.2. *Effect of the wind shielding by adjacent buildings*

In the further step of the analysis, the office building is subjected to night cooling for natural ventilation. The influence of wind shielding is first evaluated as the variation of the ventilation rates and ventilation heat losses during the night due to the presence of the surrounding buildings. Night-ventilation rates are calculated with the AFN model using the wind pressure coefficients measured by Quan et al. [27,28] at different floor heights and PAD values. Both the Air Changes per Hour (ACH_N) and the heat losses for night-ventilation (Q_V) are estimated for different zones. The seasonal-averaged ACH_N and the seasonal Q_V values in Amsterdam, Milan and Rome are shown in Fig. 7. Note that in Table 5 both the mean value at the floor elevation and the standard deviation due to different thermal zones are illustrated.

As it happens for the solar energy transmitted through the windows, the impact of the PAD on the ACH_N is generally higher at the 2nd floor than at the 5th floor. The difference in the natural ventilation rates between the two floors is maximum for PAD = 0.3 and tends to decrease at PAD = 0.6 (Fig. 7). At PAD = 0.1, the wind shielding effect is modest and the ACH_N as compared to the values for the isolated building are reduced by 9% (AM), 17% (MI) and 14% (RO) at the 2nd floor and by 6% (AM), 14% (MI) and 11% (RO) at the 5th floor. A more relevant impact is found at PAD = 0.3 and 0.6. At PAD = 0.6 the ACH_N are reduced by 74% (AM), 88% (MI) and 79% (RO) at the 2nd floor, and by 72% (AM), 85% (MI) and 79% (RO) at the 5th floor. The greatest sensitivity of the ventilation rates to the PAD is thus found for Milan, followed by Rome and Amsterdam. Considering that for the isolated building the ACH_N at the 2nd floor are equal to 1.0 h^{-1} (MI), 4.7 h^{-1} (RO) and 6.1 h^{-1} (AM), it can be remarked that the sensitivity is higher where the natural ventilation rates are lower.

Ventilation losses during the night are influenced on the one side by the natural ventilation rates across the zones and on the other side by the temperature difference between the zones and the outdoor. By looking at the ventilation losses Q_v in the three locations (Fig. 7, Table 5), it can be noticed that Amsterdam has the highest potential for night cooling by natural ventilation, resulting from high ventilation rates and low outdoor temperatures during the night (Table 2). In turn in Milan Q_v are very small, since both ventilation rates are small and night outdoor temperatures are high (Table 2). An intermediate situation is found in Rome, where high ventilation rates but also high outdoor temperatures (Table 2) are found. The impact of the PAD on the ventilation losses is found to be higher in Rome, followed by Amsterdam and Milan. For instance Q_V at the 2nd floor obtained at PAD 0.6 compared to the isolated building is reduced by 52% (RO), 50% (AM) and 33% (MI). It can be remarked then that the impact of the PAD on the ventilation losses is higher in the locations where the ventilation rates play a major role in the effectiveness of night ventilation.

Table 5
Night-averaged Air Changes per Hour (ACH_N) and ventilation losses (Q_V) for the ventilated building obtained with different PAD, locations and floor elevation (mean values and standard deviations over the thermal zones).

		Baseline case								Simplified UHI scenario							
		ACH_N [h^{-1}]				Q_V [kWh/m^2]				ACH_N [kWh/m^2]				Q_V [kWh/m^2]			
		ACH_{N-2}		ACH_{N-5}		Q_{V-2}		Q_{V-5}		ACH_{N-2}		ACH_{N-5}		Q_{V-2}		Q_{V-5}	
		Mean	SD	Mean	SD	Mean	SD	Mean	SD	Mean	SD	Mean	SD	Mean	SD	Mean	SD
AM	isolated	6.1	1.0	6.3	1.0	18.0	8.5	18.2	8.6	–	–	–	–	–	–	–	–
	PAD 0.1	5.5	0.8	5.9	0.8	16.8	8.9	17.4	8.8	–	–	–	–	–	–	–	–
	PAD 0.3	3.1	0.5	4.0	–	12.6	7.4	14.6	8.4	3.4	0.8	4.4	0.8	10.3	6.5	12.1	7.4
	PAD 0.6	1.6	0.4	1.8	0.5	8.9	3.6	10.4	5.3	1.7	0.4	1.8	0.5	7.0	3.0	8.3	4.4
MI	isolated	1.0	0.3	1.1	0.3	8.9	3.6	9.0	3.7	–	–	–	–	–	–	–	–
	PAD 0.1	0.8	0.2	1.0	0.2	8.4	3.5	8.6	3.6	–	–	–	–	–	–	–	–
	PAD 0.3	0.3	0.1	0.6	0.1	7.2	3.0	7.7	3.2	0.3	0.1	0.6	0.1	5.0	2.2	5.5	2.4
	PAD 0.6	0.1	0.0	0.2	0.0	6.0	2.1	6.7	2.5	0.1	0.0	0.2	0.0	4.1	1.4	4.6	1.8
RO	isolated	4.7	0.5	5.1	0.5	10.0	4.8	10.2	5.0	–	–	–	–	–	–	–	–
	PAD 0.1	4.1	0.6	4.5	0.5	9.2	5.0	9.6	4.9	–	–	–	–	–	–	–	–
	PAD 0.3	2.0	0.4	2.7	0.4	6.7	3.9	7.7	4.4	2.0	0.4	2.7	0.4	4.4	2.8	5.1	3.3
	PAD 0.6	1.0	0.3	1.1	0.3	4.8	1.9	5.3	2.4	1.0	0.3	1.1	0.3	2.9	1.3	3.4	1.6

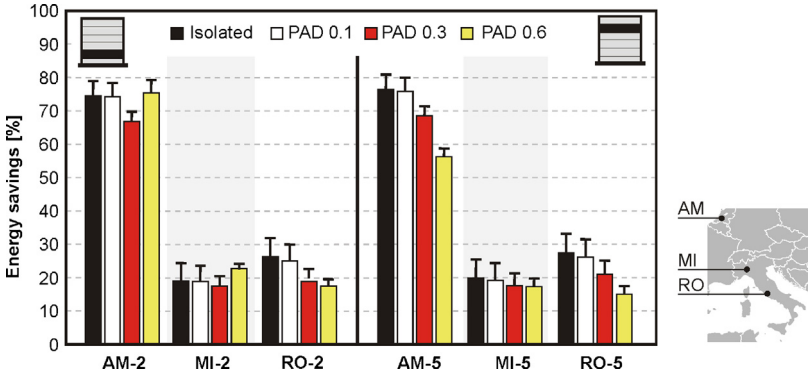

Fig. 8. Energy savings of the 2nd (left) and 5th (right) floor for different PAD in Amsterdam (AM), Milan (MI) and Rome (RO). Error bars represent the standard deviation over the zones.

3.3. *Impact of the urban environment on the energy saving due to natural night ventilation*

The energy savings for natural night-ventilation are calculated as the difference between the cooling energy demand of the unventilated ($Q_{C,UV}$) and the night-ventilated ($Q_{C,V}$) building, with respect to $Q_{C,UV}$. Results are reported in Table 6 (as mean values over the zones) and shown in Fig. 8 for different PAD, floor elevation and location (reporting the mean values and the standard deviation over the zones as error bars).

Results show that solar shading and wind shielding by adjacent buildings have a counteracting effect on the cooling energy performance of the reference building but the prevailing effect is strongly case-dependent. At the higher floor elevations, despite the reduction of the cooling demand with the increase of PAD, the drop in the ventilation rate causes a significant reduction of the energy savings for night-ventilation. For instance, due to the increase of PAD from 0 to 0.6, the energy savings at the 5th floor in Amsterdam are reduced from 76% to 56%, in Milan from 20% to 18%, and in Rome from 28% to 15%. Nevertheless, it can be remarked that at the 2nd floor in Amsterdam and Milan a minimum of the energy savings is found for PAD = 0.3. This outcome may be explained by analyzing the reduction of $Q_{C,UV}$ and ACH_N with the PAD for the 2nd and the 5th floor in Amsterdam. Fig. 9 shows the variation of the ratios $Q^*_{C,UV}$ ($Q_{C,UV}$ at a given PAD over $Q_{C,UV}$ for the isolated building) and ACH^*_N (ACH_N at a given PAD over ACH_N for the isolated building). Some observation can be made from the slopes of the graphs of $Q^*_{C,UV}$ and ACH^*_N. At the 5th floor the slope of $Q^*_{C,UV}$ for both the intervals between PAD 0.1 and 0.3 and between 0.3 and 0.6 is smaller than the slope of ACH^*_N. This means that as the PAD increases, the night ventilation rates decrease more rapidly than the cooling demand. Therefore a reduction of the energy savings with the PAD can be expected. However, at the 2nd floor the slope of $Q^*_{C,UV}$ is smaller than the slope of ACH^*_N for the interval between PAD 0.1 and 0.3 and higher for the interval between PAD 0.3 and 0.6. Thus, as the PAD increases from 0.3 to 0.6, the cooling demand decreases more rapidly than the night ventilation rates. As a consequence, the energy savings decrease when the PAD increases from 0.1 to 0.3 and increase when the PAD increases from 0.3 to 0.6. Similar considerations can be derived for Milan.

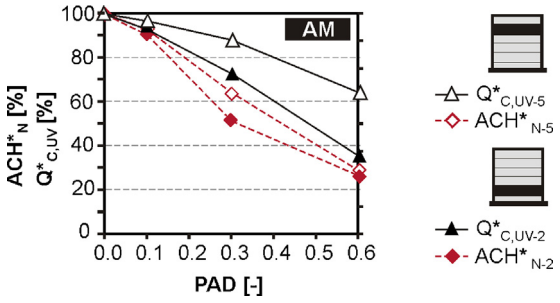

Fig. 9. Ratios $Q^*_{C,UV}$ ($Q_{C,UV}$ at a given PAD over $Q_{C,UV}$ for the isolated building) and ACH^*_N (ACH_N at a given PAD over ACH_N for the isolated building) versus PAD for the 2nd and the 5th floor in Amsterdam.

When the results for the three locations are analyzed, it can be noted that in Amsterdam, where the suitability to night cooling is the highest, night-ventilation is an effective cooling strategy even at very high PAD. In Milan the effect of the PAD on the modest energy saving potential for night-ventilation is almost negligible. On the contrary, in Rome the energy savings for night-ventilation are almost halved.

Fig. 10 shows the results obtained with the albedo 0.7 and simplified UHI scenarios on the energy savings for PAD = 0.3 and 0.6. In Fig. 10 the mean values over the zones are shown as well as the standard deviation as error bars. Overall, a higher albedo of the surrounding buildings equal to 0.7 leads to lower energy savings. At the 5th floor for PAD = 0.6 the energy savings are reduced to 51% in Amsterdam, 16% in Milan and 14% in Rome (Table 6). This happens because the higher albedo reduces the dependency of $Q_{C,UV}$ on the

Table 6
Energy savings obtained with different PAD, locations and floor elevation for the baseline case and for the albedo 0.7 and the simplified UHI scenarios (mean values over the thermal zones).

		Energy savings (2nd floor) [%]			Energy savings (5th floor) [%]		
		AM-2	MI-2	RO-2	AM-5	MI-5	RO-5
Baseline case	Isolated	75%	20%	26%	76%	20%	28%
	PAD 0.1	74%	19%	25%	76%	19%	26%
	PAD 0.3	67%	18%	19%	68%	18%	21%
	PAD 0.6	76%	23%	18%	56%	18%	15%
Albedo 0.7 scenario	PAD 0.3	63%	17%	18%	65%	17%	20%
	PAD 0.6	69%	21%	17%	51%	16%	14%
Simplified UHI scenario	PAD 0.3	56%	12%	12%	58%	12%	14%
	PAD 0.6	62%	16%	11%	44%	12%	9%

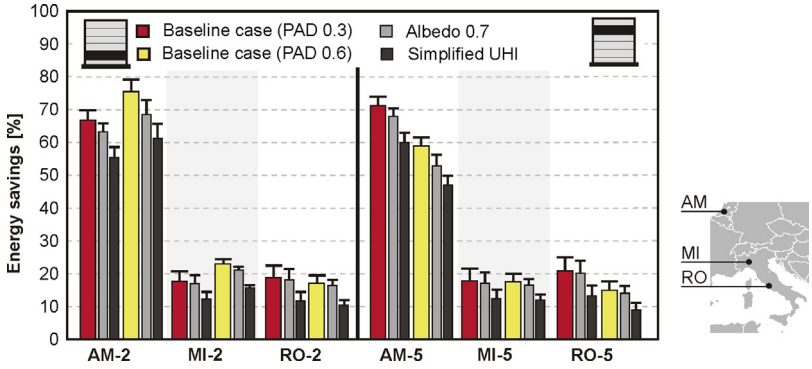

Fig. 10. Energy savings of the 2nd (left) and 5th (right) floor of the reference building obtained at PAD = 0.3 and 0.6 for the baseline case and for the albedo 0.7 and the simplified UHI scenarios (ΔT_{db} = 3 °C). Error bars represent the standard deviation over the zones.

PAD (Fig. 6, Table 4). As regards to the simplified UHI scenario, it can be noted that the UHI affects not only $Q_{C,UV}$ (Fig. 6, Table 4), but also the cooling effectiveness of night-ventilation, by reducing the night indoor-outdoor temperature difference. In fact, at the 5th floor the energy savings for PAD = 0.6 are reduced to 44%, 12% and 9% in Amsterdam, Milan and Rome respectively (Fig. 10, Table 6).

4. Conclusions

In the present study the impact of the urban environment on the effectiveness of natural night-ventilation for an office building is assessed. The building is placed in urban areas of increased Plan Area Density, and the cooling energy demand and savings are calculated for three European locations with different suitability to night-cooling using EnergyPlus and the embedded AFN model. Both wind shielding and solar shading effect of surrounding buildings are considered. Experimental wind pressure coefficients are used in the AFN model to estimate the variation of the wind pressure on the facades of the reference building. The reduction of solar gains is taken into account by describing the adjacent buildings as shading surfaces. The sensitivity of the energy performance to the albedo of the surrounding buildings is also tested as well as the impact of a simplified UHI scenario.

Overall, it is shown that solar shading and the wind shielding by surrounding buildings have a counteracting effect on the cooling energy savings for night-ventilation, and that the dominant effect may vary across situations. The results for the three locations analyzed show a significant reduction of the energy savings in high-density urban environments for the high floor elevations. For instance, the energy savings calculated for the isolated case and for the case of PAD = 0.6 at the 5th floor of the building decrease from 76% to 56% in Amsterdam, from 20% to 18% in Milan and from 28% to 15% in Rome. This reduction is proved to be more pronounced if the Urban Heat Island effect is taken into account leading to energy savings of 44%, 12% and 9% for Amsterdam, Milan and Rome respectively.

In turn, predicting the dominant effect for the low floor elevations is less obvious: in Amsterdam and Milan a minimum of the energy savings at the 2nd floor was found for PAD = 0.3. In these cases in fact the cooling demand decreases more rapidly than the night ventilation rates as the PAD increases from 0.3 to 0.6. Thus, the analysis has shown that a correct assessment of the effectiveness of natural night-ventilation in the urban environment is inseparable from considering both the solar shading effect and the wind shielding of adjacent buildings. In fact, only the investigation of the combined behavior of such aspects allows an accurate prediction of the final energy saving potential of natural night-ventilation for a given location.

These outcomes are clearly limited to the case study analyzed, consisting of a low-rise building placed in regular distributions of simplified surrounding buildings. For more complex building geometries or urban patterns, experimental pressure coefficients might not be available, limiting the accuracy of the predicted ventilation rates. For this reason, the use of non-experimental pressure coefficient values could produce misleading results and alter the sensitivity of the energy savings to the urban environment.

Finally, the study demonstrates that BES/AFN tools allow modeling the main effects of the urban environment on the energy performance of a building, but also that an accurate description of the urban environment is crucial to design effective passive cooling solutions.

References

[1] M. Santamouris, D. Asimakopoulos, Passive Cooling of Buildings, Earthscan/James & James, London, UK, 1996.
[2] V. Geros, M. Santamouris, S. Karatasou, A. Tsangrassoulis, N. Papanikolaou, On the cooling potential of night ventilation techniques in the urban environment, Energy and Buildings 37 (2005) 243–257.
[3] M. Kolokotroni, B.C. Webb, S.D. Hayes, Summer cooling with night ventilation for office buildings in moderate climates, Energy and Buildings 27 (1998) 231–237.
[4] N. Artmann, H. Manz, P. Heiselberg, Parameter study on performance of building cooling by night-time ventilation, Renewable Energy 33 (2008) 2589–2598.
[5] C.A. Balaras, The role of thermal mass on the cooling load of buildings. An overview of computational methods, Energy and Buildings 24 (1996) 1–10.
[6] T.R. Oke, G.T. Johnson, D.G. Steyn, I.D. Watson, Simulation of surface urban heat islands under ideal conditions at night part 2: diagnosis of causation, Boundary Layer Meteorology 56 (1991) 339–358.
[7] N. Artmann, H. Manz, P. Heiselberg, Climatic potential for passive cooling of buildings by night-time ventilation in Europe, Applied Energy 84 (2007) 187–201.
[8] M. Grosso, Wind pressure distribution around buildings: a parametrical model, Energy and Buildings 18 (1992) 101–131.
[9] G. van Moeseke, E. Gratia, S. Reiter, A. De Herde, Wind pressure distribution influence on natural ventilation for different incidences and environment densities, Energy and Buildings 37 (2005) 878–889.
[10] C.N. Hewitt, A.V. Jackson, Atmospheric science for environmental scientists, Wiley. com, 2009.
[11] T.R. Oke, Street design and urban canopy layer climate, Energy and Buildings 11 (1988) 103–113.
[12] C.S.B. Grimmond, T.R. Oke, Aerodynamic properties of urban areas derived from analysis of surface form, Journal of Applied Meteorology 38 (1999) 1262–1292.
[13] L. Gu, Airflow network modeling in EnergyPlus, in: 10th International Building Performance Simulation Association Conference and Exhibition, 2007, pp. 964–971.
[14] J.L.M. Hensen, R. Lamberts, Building Performance Simulation for Design and Operation, Routledge, London, 2011.
[15] J. Axley, Multizone airflow modeling in buildings: history and theory, HVAC&R Research 13 (2007) 907–928.
[16] D.B. Crawley, Estimating the impacts of climate change and urbanization on building performance, Journal of Building Performance Simulation 1 (2008) 91–115.
[17] T. Kershaw, M. Sanderson, D. Coley, M. Eames, Estimation of the urban heat island for UK climate change projections, Building Services Engineering Research Technologies 31 (2010) 251–263.

[18] D. Costola, B. Blocken, J.L.M. Hensen, Overview of pressure coefficient data in building energy simulation and airflow network programs, Building and Environment 44 (2009) 2027–2036.
[19] D. Costola, B. Blocken, M. Ohba, J. Hensen, Uncertainty in airflow rate calculations due to the use of surface-averaged pressure coefficients, Energy and Buildings 42 (2010) 881–888.
[20] R. Ramponi, A. Angelotti, B. Blocken, Energy saving potential of night-ventilation: Sensitivity to pressure coefficients, Applied Energy 123 (2014) 185–195.
[21] T. Schulze, U. Eicker, Controlled natural ventilation for energy efficient buildings, Energy and Buildings 56 (2013) 221–232.
[22] P. Bhiwapurkar, D. Moschandreas, Street geometry and energy conservation of urban buildings in Chicago, Intelligent Buildings International 2 (2010) 233–250.
[23] S. Nikoofard, V.I. Ugursal, I. Beausoleil-Morrison, Effect of external shading on household energy requirement for heating and cooling in Canada, Energy and Buildings 43 (2011) 1627–1635.
[24] A. Tereci, S.T.E. Ozkan, U. Eicker, Energy benchmarking for residential buildings, Energy and Buildings 60 (2013) 92–99.
[25] DOE, EnergyPlus Engineering reference, (2010).
[26] S. Dutton, L. Shao, S. Riffat, Validation and parametric analysis of EnergyPlus: air flow network model using contam, SimBuild (2008) 124–131.
[27] Y. Quan, Y. Tamura, M. Matsui, S. Cao, A. Yoshida, S. Xu, Interference effect of a surrounding building group on wind loads on flat roof of low-rise building: Part I, Distribution of local wind pressure coefficient, Wind Engineers, JAWE 32 (2007) 211–212.
[28] Y. Quan, Y. Tamura, M. Matsui, S. Cao, A. Yoshida, S. Xu, Interference effect of a surrounding building group on wind loads on flat roof of low-rise building: Part II, Interference factor of worst extreme local and area-averaged suction pressure coefficients, Wind Engineers, JAWE 32 (2007) 213–214.
[29] CEN, EN ISO 13786: Thermal Performance of Building Components – Dynamic Thermal Characteristics – Calculation Methods, (2007).
[30] N. Aste, A. Angelotti, M. Buzzetti, The influence of the external walls thermal inertia on the energy performance of well insulated buildings, Energy and Buildings 41 (2009) 1181–1187.
[31] M. Rossi, V.M. Rocco, M. Buzzetti, External walls design: The role of periodic thermal transmittance and internal areal heat capacity, Energy and Buildings 68-C (2014) 732–740.
[32] Ente Nazionale Italiano di Unificazione (UNI), UNI/TS 11300-1: Energy performance of buildings Part 1: Evaluation of energy need for space heating and cooling, (2008).
[33] Architectural Institute of Japan (AIJ), Recommendations for loads on buildings, (2004).
[34] ASHRAE, International Weather for Energy Calculations (IWEC Weather Files), (2001).
[35] CIBSE, Guide A: Environmental Design, The Chartered Institution of Building Services Engineers, London, 1999.
[36] ASHRAE, Handbook of Fundamentals, American Society of Heating Refrigerating and Air Conditioning Engineers, Atlanta, GA, 2005.